# Mechanisms of aortic carboxypeptidase-like protein secretion and identification of an intracellularly retained variant associated with Ehlers–Danlos syndrome

Received for publication, April 15, 2020, and in revised form, May 28, 2020 Published, Papers in Press, June 1, 2020, DOI 10.1074/jbc.RA120.013902

**Neya Vishwanath[1,‡], William J. Monis[1,‡], Gwendolyn A. Hoffmann[2], Bhavana Ramachandran[1], Vincent DiGiacomo[1], Joyce Y. Wong[2], Michael L. Smith[2], and Matthew D. Layne[1,*]**

*From the [1]Department of Biochemistry, Boston University School of Medicine, Boston, Massachusetts, USA and the [2]Department of Biomedical Engineering, Boston University, Boston, Massachusetts, USA*

Edited by Gerald W. Hart

**Aortic carboxypeptidase-like protein (ACLP) is a collagen-binding extracellular matrix protein that has important roles in wound healing and fibrosis. ACLP contains thrombospondin repeats, a collagen-binding discoidin domain, and a catalytically inactive metallocarboxypeptidase domain. Recently, mutations in the ACLP-encoding gene, AE-binding protein 1 (*AEBP1*), have been discovered, leading to the identification of a new variant of Ehlers–Danlos syndrome causing connective tissue disruptions in multiple organs. Currently, little is known about the mechanisms of ACLP secretion or the role of post-translational modifications in these processes. We show here that the secreted form of ACLP contains *N*-linked glycosylation and that inhibition of glycosylation results in its intracellular retention. Using site-directed mutagenesis, we determined that glycosylation of Asn-471 and Asn-1030 is necessary for ACLP secretion and identified a specific N-terminal proteolytic ACLP fragment. To determine the contribution of secreted ACLP to extracellular matrix mechanical properties, we generated and mechanically tested wet-spun collagen ACLP composite fibers, finding that ACLP enhances the modulus (or stiffness), toughness, and tensile strength of the fibers. Some *AEBP1* mutations were null alleles, whereas others resulted in expressed proteins. We tested the hypothesis that a recently discovered 40-amino acid mutation and insertion in the ACLP discoidin domain regulates collagen binding and assembly. Interestingly, we found that this protein variant is retained intracellularly and induces endoplasmic reticulum stress identified with an XBP1-based endoplasmic reticulum stress reporter. Our findings highlight the importance of *N*-linked glycosylation of ACLP for its secretion and contribute to our understanding of ACLP-dependent disease pathologies.**

The structural integrity and mechanical properties of tissues are regulated by the extracellular matrix (ECM). Perturbations in the ECM contribute to fibrosis, cancer, and cardiovascular disease progression (1–4). The reduction in ECM synthesis and dysfunctional assembly is also the underlying cause of the morbidity observed in individuals with impaired wound healing and in those with genetic connective tissue disorders, including the Ehlers–Danlos syndromes (EDS) (5, 6). Individuals with EDS-causing mutations in collagen or collagen regulatory proteins display a disease spectrum that includes aberrant wound healing, joint hypermobility, and vascular disruption, all related to a mechanically weak or fragile ECM (5). Mutations in genes encoding collagens I, III, and V lead to irregularities in collagen primary structure, processing, folding, and cross-linking (5, 6).

Recently, several groups have identified EDS-causative mutations in the *AEBP1* gene, which encodes the ECM protein aortic carboxypeptidase-like protein (ACLP) (7–11). These compound heterozygous or homozygous *AEBP1*/ACLP mutations cause a distinct EDS subtype, designated EDS classic-like 2 (EDSCLL2). Individuals with *AEBP1*/ACLP mutations suffer from severe connective tissue pathologies including common and variable features. ACLP mutations in humans result in delayed wound healing, abnormal scarring, joint hypermobility, hip dislocations, osteopenia, mitral valve prolapse, dilatation of the aortic root, and aortic dissection (7–11). These symptoms are also observed in classical, hypermobile, cardiac-valvular, vascular, musculocontractural, and kyphoscoliotic EDS (11).

The gene name *AEBP1* (adipocyte enhancer–binding protein 1) is derived from a mouse cDNA that was proposed to be a transcriptional repressor (12). Compared with ACLP, the mouse Aebp1 cDNA is missing ~1.5 kb of sequence (encoding more than 400 amino acids), and it does not likely encode for an authentic protein (13–17). Consistent with a role in the extracellular environment, ACLP contains a signal peptide, an N-terminal domain predicted to fold into thrombospondin type I repeats, a central collagen-binding discoidin domain, and a C-terminal catalytically inactive metallocarboxypeptidase domain (8, 13–15). Supporting the concept that ACLP functions in collagen assembly and regulatory pathways, ACLP is expressed in collagen-rich connective tissues, including the vasculature, skin, tendons, and ligaments (18, 19). Our previous studies determined that loss of ACLP function in mice resulted in delayed dermal wound healing and provided protection in the lung against a profibrotic injury (18, 20). We showed that the central discoidin domain of ACLP bound to fibrillar collagens *in vitro* (8).

In addition to its roles in the ECM, ACLP modulates signal transduction pathways and enhances the transforming growth factor $\beta$ (TGF$\beta$) receptor–signaling pathway, leading to

‡These authors contributed equally to this work.
*For correspondence: Matthew D. Layne, mlayne@bu.edu.
Present address for William J. Monis: Sanofi, Cambridge, Massachusetts, USA.
Present address for Vincent DiGiacomo: DeepBiome Therapeutics, Cambridge, Massachusetts, USA.

activation of lung myofibroblast differentiation (21). The ACLP-dependent pathway is also important in the regulation of adipose progenitor differentiation (22). Furthermore, a recent study determined that in response to high-fat diet, hepatic stellate cell–derived ACLP stimulated the Wnt-$\beta$-catenin pathway through the binding and activation of the Frz8/Lrp6 complex, which exacerbates nonalcoholic steatohepatitis (17).

Despite these functions for ACLP in multiple diseases, including fibrosis and EDS, currently very little is known about the mechanisms of ACLP processing and post-translational modifications that result in secretion of ACLP into the extracellular environment. The goal of the present study was to characterize the post-translational processing and secretion of ACLP. Based on accumulating evidence that biallelic mutations in *AEBP1* cause a distinct EDS subtype (EDSCLL2), we examined the contribution of ACLP to collagen fiber mechanical properties and discovered that at least one EDS-causing mutation in ACLP generates an expressed protein that is retained within the secretory pathway.

## Results

### *Characterization of secreted ACLP isoforms*

ACLP contains a signal peptide, thrombospondin repeats, a collagen-binding discoidin domain, and a catalytically inactive carboxypeptidase domain (Fig. 1*A*). Prior work determined that ACLP is retained in the ECM and co-localizes with collagen in multiple connective tissues (18, 19); however, the mechanisms controlling ACLP secretion are unknown. Because ACLP expression is activated by vascular injury (13) and humans with *AEBP1*/ACLP mutations exhibit vascular complications (9, 11), we used cultured mouse aortic smooth muscle cells (SMC) as a model system to investigate the regulation of ACLP processing and secretion. SMC were initially plated at low density ($1.5 \times 10^5$ cells/cm$^2$) and cultured over 7 days in proliferative conditions. Total cell lysates were extracted at 0-, 2-, 5-, and 7-day time points, and samples were analyzed for ACLP expression by Western blotting using an antibody generated against mouse ACLP (amino acids 615-1128) (13). ACLP expression increased with time in culture, and a "thickened" upper band with slower mobility became apparent at later time points (Fig. 1*B*, *top arrow*).

To examine the nature of the upper ACLP band (Fig. 1*B*), we cultured cells for 2 days with or without ascorbic acid, which is required for collagen synthesis and secretion (23, 24). Total cell lysates and media samples were collected and analyzed for ACLP expression by Western blotting. To increase the resolution of the gels and to define the nature of these ACLP bands, we decreased the percentage of acrylamide. Total cell lysates from the control and ascorbic acid–treated cells contained two distinct bands (Fig. 1*C*, *arrows*). Only the larger band was detected in the media samples, suggesting that this is the secreted form of ACLP. This band was evident both with and without ascorbic acid treatment (Fig. 1*C*).

### *Inhibition of ACLP glycosylation prevents secretion*

To examine whether the larger, secreted form of ACLP is the result of post-translational modification (glycosylation), we

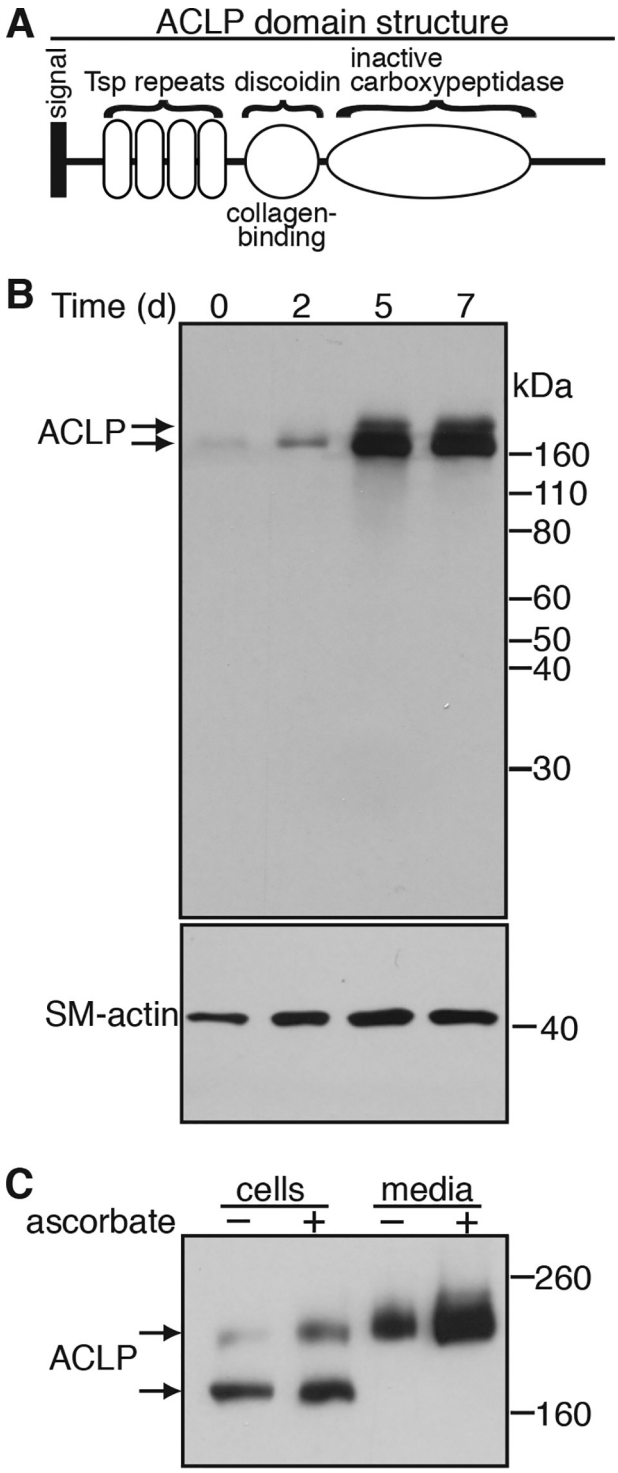


**Figure 1. Characterization of ACLP production and secretion.** *A*, ACLP domain structure: N-terminal signal peptide, thrombospondin (*Tsp*) repeats, collagen-binding discoidin domain, catalytically inactive carboxypeptidase domain. *B*, mouse aortic SMC were plated at a density of $1.5 \times 10^5$ cells/cm$^2$, and total protein lysates were collected after 0, 2, 5, and 7 days from initial seeding. Protein extracts (20 μg) were analyzed by Western blotting (4–20% SDS-PAGE) for ACLP (*arrows*) and smooth muscle actin (*SM-actin*). *C*, SMC were plated at a density of $5 \times 10^5$ cells/cm$^2$ and incubated overnight, treated with or without 50 μg/ml 2-phospho-L-ascorbic acid for 24 h. The cells were then washed twice with serum-free medium and then incubated in the same 2-phospho-L-ascorbic acid treatments for an additional 24 h in serum-free conditions. Total cell lysates and media samples were run on a 6% SDS-polyacrylamide gel and blotted for ACLP.

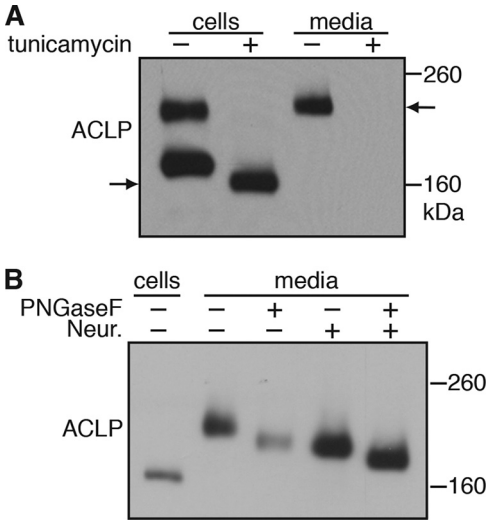


**Figure 2. ACLP undergoes *N*-linked post-translational modifications.** SMC were cultured to confluence and then treated with tunicamycin (2 μg/ml) or vehicle control (DMSO) for 24 h. The cells were then washed twice with serum-free medium and then incubated with or without tunicamycin for an additional 24 h in serum-free conditions. *A*, samples were run on 6% SDS-polyacrylamide gels, and Western blots were probed with ACLP antibodies. *B*, total cell lysate and medium collected from SMC were digested with or without PNGase F or neuraminidase (*Neur.*) and analyzed by Western blotting for ACLP.

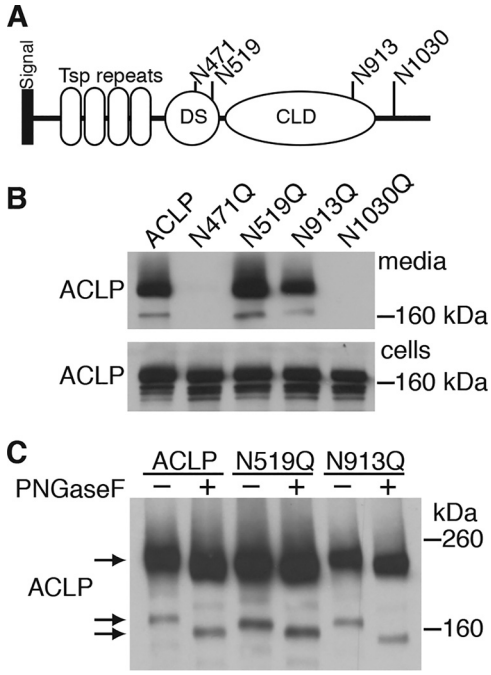


**Figure 3. Identification of ACLP *N*-linked glycosylation residues that are required for secretion.** *A*, localization of predicted ACLP *N*-linked glycosylation sites. Shown are N-terminal signal sequence, thrombospondin repeats, discoidin-like domain (*DS*), and carboxypeptidase-like domain (*CLD*) containing four asparagine to glutamine point mutations. *B*, AD-293 cells were plated at a density of $2 \times 10^5$ cells/cm$^2$ and incubated overnight. Cells were then transfected with either ACLP or ACLP N/Q mutants (N471Q, N519Q, N913Q, or N1030Q) for 24 h. Cells washed three times with serum-free medium and incubated in serum-free conditions for an additional 24 h. Total cell lysates were normalized to 10 μg, and medium was normalized to 5 μl of input volume. Samples were run on a 4–20% SDS-polyacrylamide gel and blotted for ACLP. *C*, media from AD-293 cells transfected with either WT ACLP or ACLP N/Q mutants N519Q and N913Q were digested with or without PNGase F for 1 h at 37 °C. Samples were run on a 6% SDS-polyacrylamide gel and blotted for ACLP.

treated SMC with 2 μg/ml tunicamycin or DMSO vehicle control for 24 h and isolated total cell lysates and media samples. Tunicamycin inhibits UDP-GlcNAc:dolichol phosphate GlcNAc-1-P transferase, which catalyzes the first step in protein glycosylation (25) and prevents proteins from undergoing *N*-linked glycosylation. Treatment with tunicamycin increased the mobility of ACLP in total cell lysates and resulted in a single band (Fig. 2*A*, *left arrow*), demonstrating that ACLP contains *N*-linked glycosylation. ACLP was not detected in the media samples from the tunicamycin-treated cultures, indicating that *N*-linked glycosylation was required for ACLP secretion (Fig. 2*A*, *right arrow*).

### *Post-translational modification of ACLP*

To characterize the post-translational modifications of secreted ACLP, we treated SMC media samples with peptide:*N*-glycosidase F (PNGase F) and/or neuraminidase. PNGase F cleaves between the innermost GlcNAc and asparagine residues of high-mannose, hybrid, and complex oligosaccharides from *N*-linked glycoproteins; neuraminidase cleaves sialic acid residues. Increases in ACLP mobility were observed in PNGase F– and neuraminidase–treated samples (Fig. 2*B*), with a greater increase in mobility with the simultaneous treatment with PNGase F and neuraminidase. These findings are consistent with the presence of *N*-linked glycosylation on ACLP.

### *Identification of ACLP N-linked glycosylation sites*

To identify the sites on ACLP that undergo *N*-linked glycosylation events, we analyzed the ACLP sequence using the NetNGlyc 1.0 server, which examines the sequence context of N*X*(S/T)) amino acid residues. Four asparagine residues were predicted to undergo *N*-linked glycosylation (mouse ACLP Asn-471, Asn-519, Asn-913, and Asn-1030) (Fig. 3*A*). These sites are conserved residues in human ACLP (Asn-480, Asn-528, Asn-922, and Asn-1039). Two predicted glycosylation sites reside in the discoidin domain (Asn-471/480, Asn-519/528); one is in the carboxypeptidase domain (Asn-913/922), and one is at the C terminus (Asn-1030/1039) (Fig. 3*A*). To examine the importance of these asparagine residues, we generated mouse ACLP expression vectors and mutated each of these residues to glutamine (26). Mutations are designated N471Q, N519Q, N913Q, and N1030Q (Fig. 3*A*). The WT and mutated ACLP constructs were transfected into AD-293 cells, and total cell lysates and media samples were examined for ACLP expression by Western blot analysis. Interestingly, ACLP mutants N471Q and N1030Q were not found in the media samples (Fig. 3*B*), although all ACLP N/Q mutants were expressed at approximately equal levels in the total cell lysates (Fig. 3*B*). These results indicate that glycosylation of Asn-471 and Asn-1030 residues is essential for ACLP secretion. To assess the glycosylation state of the ACLP mutants N519Q and N913Q, media samples that contained secreted ACLP were digested with or without PNGase F. Both the N519Q and N913Q secreted ACLP mutants decreased in size when digested with PNGase F compared with controls (Fig. 3*C*). These results support the conclusion that glycosylation of ACLP amino acid residues Asn-519 and Asn-913 was not required for ACLP secretion, but *N*-linked

glycosylation of other residues (potentially Asn-471 and Asn-1030) appears to be necessary for secretion. A smaller secreted glycosylated form of ACLP was detected in the transfected AD-293 cells (Fig. 3*C*, *bottom arrow*), potentially indicative of proteolytic processing of ACLP.

### Proteolytic processing of ACLP

In some studies, particularly those with very high ACLP levels, we observed smaller ACLP bands in the media samples of both SMC and transfected cells (Fig. 3*C*). This phenomenon was also observed recently by others (17). To examine the nature of ACLP processing, we isolated cells and media from SMC (treated with tunicamycin). In addition to the major ACLP band detected in the media, we observed an ~150 kDa band when probed with ACLP antibodies against amino acids 615-1128 (Fig. 4*A*). This result could indicate that ACLP is proteolytically cleaved prior to amino acid 615. Because sensitive and specific antibodies against the N terminus of ACLP are not available, we generated an expression vector and inserted a FLAG epitope tag directly after the predicted signal peptide cleavage site and added a Myc epitope tag at the C terminus of the protein (Fig. 4*B*). This construct was transfected into AD-293 cells, and protein lysates were analyzed by Western blotting. Analysis of the media with the FLAG antibody showed that the N-terminal portion on ACLP is detectable at a molecular mass of ~40-50 kDa (arrow) (Fig. 4*C*). In addition, an unknown protein was observed by FLAG antibody detection in the cell lysate (Fig. 4*C*, *asterisk*). As mentioned above, potentially due to the differing antibody sensitivities, we did not observe the smaller band with the c-Myc blots. These results indicate that a portion of the ACLP secreted pool is processed into separate N-terminal and C-terminal proteins.

### Role of ACLP in collagen fiber mechanics

We recently determined that the discoidin domain of ACLP binds to multiple collagens (8). Several mutations in the *AEBP1* gene have been identified, including some in the discoidin domain (7–9, 11, 17). Whereas mutations in ACLP cause alterations in connective tissue structure and collagen fibrils, it is currently unknown whether ACLP contributes to the mechanical properties of the collagen fiber. Using a novel collagen fiber wet spinning approach (27, 28), we generated collagen I (Col I) and Col I + ACLP composite fibers. We subjected the fibers to tensile testing (Fig. 5*A*) to evaluate the contribution of ACLP to collagen fiber mechanical properties, which was extracted from stress–strain curves (Fig. 5*B*). Fiber diameters were measured before tensile testing, and a small but significant decrease in diameter was found with the addition of ACLP to Col I fibers (Fig. 5*C*). The modulus was calculated as the slope of the linear region of the stress–strain curve and was found to increase with the addition of ACLP (Fig. 5*D*). Toughness, a measure of the amount of energy the fibers can absorb before breakage, was calculated from the area under the curve, and tensile strength, the maximum stress the fiber can withstand, increased with ACLP addition (Fig. 5, *E* and *F*).

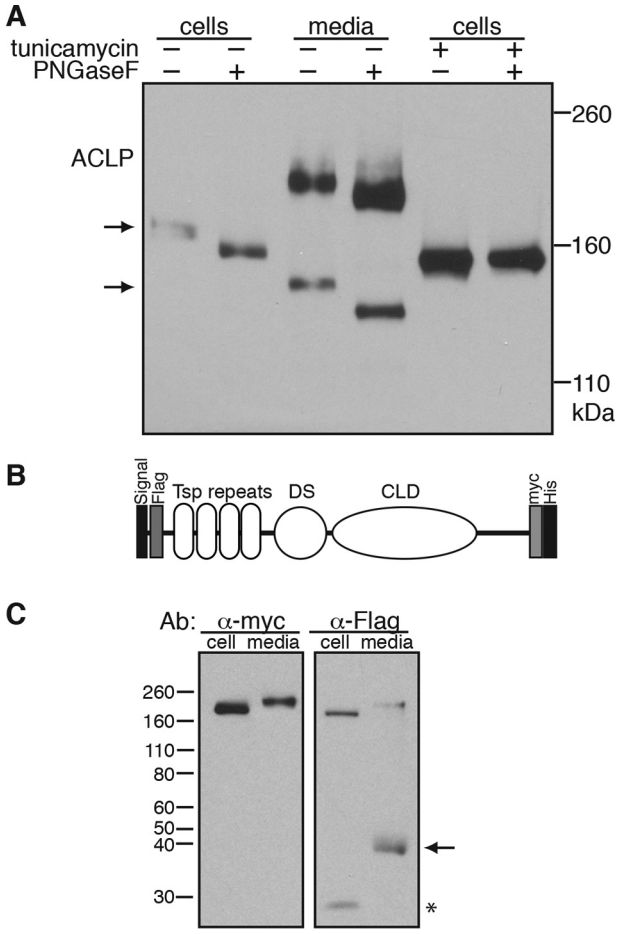


**Figure 4. ACLP undergoes proteolytic processing.** *A*, total cell lysate and medium from SMC treated with or without 2 μg/ml tunicamycin for 24 h were digested with or without PNGase F for 1 h at 37 °C. Samples were run on a 6% SDS-polyacrylamide gel and subjected to Western blotting analysis using an antibody directed against ACLP. The *bottom arrow* indicates the lower-molecular weight form of secreted ACLP in nondigested media from untreated SMC. *B*, *schematic representation* of signal-FLAG-ACLP-Myc/His from N to C termini containing a BM40 signal sequence, DYKDDDDK (FLAG) epitope, thrombospondin (*Tsp*) repeats, discoidin-like domain (*DS*), carboxypeptidase-like domain (*CLD*), c-Myc epitope, and His tag. *C*, AD-293 cells were plated at a density of $2 \times 10^5$ cells/cm$^2$ and incubated overnight. The cells were then transfected with BM40FLAGACLPMyc/His for 24 h and incubated in serum-free conditions for an additional 24 h. Total cell lysates were normalized to 12 μg, and medium was normalized to 20 μl of input volume. Samples were run on a 4–20% SDS-polyacrylamide gel and blotted for c-Myc and FLAG. *Arrow*, N-terminal cleavage; *, unidentified band.

### Characterization of the human ACLP-Ins40 mutation

We recently determined that one mutated *AEBP1* allele in an EDS patient resulted in a larger form of ACLP due to a 40-amino acid mutation and insertion in the discoidin domain (p. Asn490_Met495delins(40)) (8). This mutation is designated ACLP-Ins40 and is illustrated in Fig. 6 (*A* and *B*). Our initial goal was to test whether this mutation resulted in altered collagen binding and was responsible for changes in collagen mechanical properties. We first generated a refined homology model of the human ACLP discoidin domain mapped onto the collagen-binding domain of the discoidin domain receptor (Protein Data Bank entry 2WUH) using PyMOL (Fig. 6*C*). This mutation and insertion of 40 amino acids is not in the collagen-binding loops of the domain. To examine the function of this

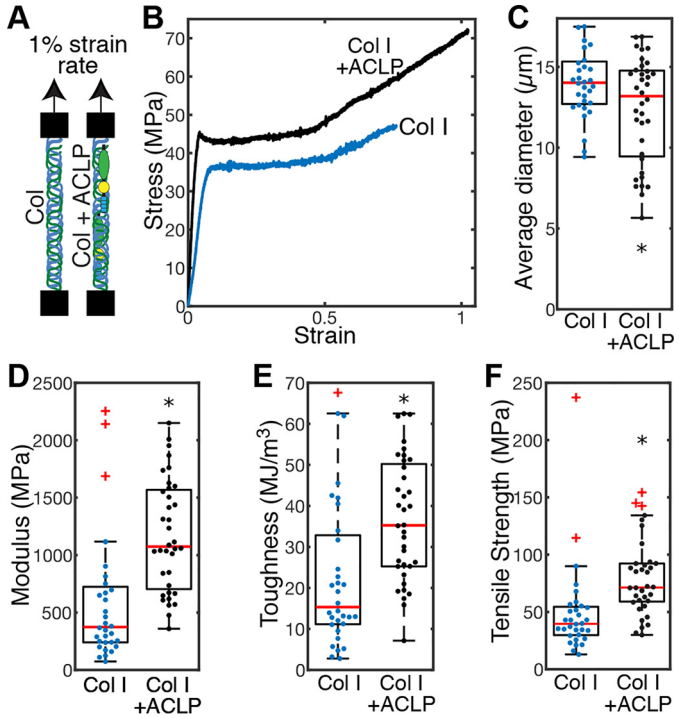


**Figure 5. ACLP improves mechanical properties of collagen fibers.** *A*, collagen and collagen + ACLP fibers were spun and mechanically tested with a 1% strain rate until breakage as described under "Experimental procedures" to obtain stress–strain curves (*B*, representative curves). *C*, fiber diameter was measured by imaging the fibers prior to testing. *D*, modulus was calculated from the slope of the linear region of the stress–strain curve. *E*, toughness was calculated from the area under the curve. *F*, tensile strength is the maximum stress attained. For *C–F*, *boxes* display the interquartile range, and *central lines* show the median. *Red plus signs*, data points located beyond the maximum *whisker* length of 1.5 times the interquartile range. Kolmogorov–Smirnov tests were performed to determine whether data fit a normal distribution. Fiber diameter, modulus, and toughness were found to fit a normal distribution, and two-sample *t* tests were performed to determine significance. Tensile strength data were not found to fit a normal distribution, so a Wilcoxon rank sum test was performed (*, $p < 0.05$).

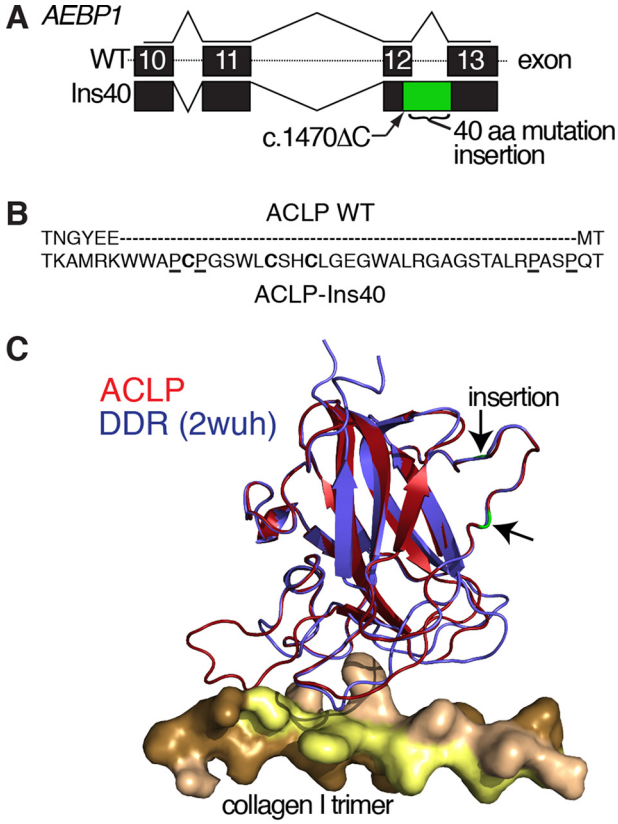


**Figure 6. Structural prediction of the ACLP-Ins40 discoidin domain mutation.** *A*, localization of the human *AEBP1* gene mutation (c.1470ΔC) that results in a 40-amino acid mutation and retention of an intron. *B*, predicted amino acid changes in ACLP-Ins40. Proline residues are *underlined*, and cysteine residues are in *boldface type*. *C*, structural prediction of the ACLP-Ins40 protein generated by a refined homology model to the discoidin domain receptor (*DDR*) discoidin domain using PyMOL. The location of the insertion is noted with *arrows*, and the margin of insertion is indicated in *green*.

ACLP mutation, we generated an expression vector harboring this mutation by PCR. Human ACLP-WT and Ins40 C-terminal FLAG epitope–tagged expression vectors were transiently transfected into AD-293 cells, and total cell lysates and media samples were collected. As anticipated, and consistent with lysates from human fibroblasts (8), the ACLP-Ins40 protein is larger due to the additional amino acids (Fig. 7*A*). Interestingly, we did not detect ACLP-Ins40 in the media samples (Fig. 7*A*), indicating that it was not secreted. We next examined whether the ACLP-Ins40 protein was retained intracellularly. Fibroblasts were chosen for these studies due to their role in collagen synthesis in connective tissue and their importance in EDS pathology. To examine whether the ACLP-Ins40 protein was retained, 3T3 fibroblasts were transiently transfected with ACLP-WT and ACLP-Ins40 expression plasmids containing a FLAG epitope tag. After 24 h, cells were fixed, permeabilized, and stained with a monoclonal Cy3-conjugated anti-FLAG antibody. Immunofluorescence microscopy revealed that both ACLP-WT and ACLP-Ins40 showed a similar perinuclear expression pattern (Fig. 7*B*) that is consistent with translocation into the ER and secretory pathway. Higher-magnification images of the ACLP-Ins40 protein revealed a pattern consistent with localization to the ER and with apparent absence in the Golgi apparatus (Fig. 7*C*).

### *Investigating ACLP-Ins40 mutation as an inducer of ER stress*

Mutations in other ECM proteins that cause connective tissue disease, including collagen VI and collagen III, induce ER stress when retained intracellularly (29). Therefore, experiments were performed to test the hypothesis that ACLP-Ins40 expression and subsequent intracellular retention trigger the unfolded protein response and activate the ER stress pathway. In cells undergoing ER stress, the XBP1 mRNA is spliced in the cytoplasm by IRE1 (30). We generated a sensor of ER stress by fusing the region of XBP1 that is spliced by IRE1 to EGFP with a nuclear localization signal. In the presence of ER stress, the activation of IRE1 is expected to splice this mRNA, leading to expression of a nucleus-localized EGFP. To validate this construct, 3T3 fibroblasts were transiently transfected with the unspliced XBP1u-EGFP plasmid for 12 h and were subsequently treated with the ER stress–inducing compound tunicamycin or thapsigargin for 15 h. Cells treated with tunicamycin or thapsigargin resulted in nuclear EGFP expression (data not shown). To test whether the ACLP-Ins40 mutant induced ER stress, 3T3 fibroblasts were co-transfected with ACLP-WT + XBP1u-EGFP

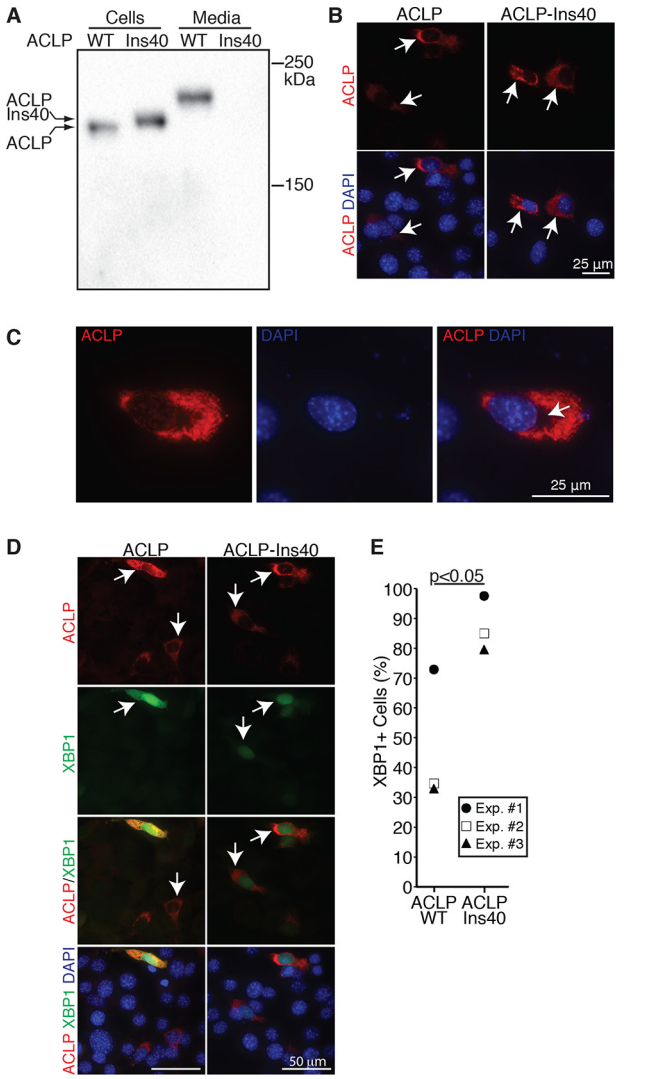


**Figure 7. ACLP-Ins40 is not secreted from cells and induces ER stress.** *A*, 293 cells were transiently transfected with pCMV6-ACLP or pCMV6-ACLP-Ins40 plasmids, and total protein and conditioned media was collected after 24 h. Western blotting was performed on 25 μg of total protein and equal volumes of 50-fold concentrated conditioned media with antibodies against ACLP. Both ACLP-WT and ACLP-Ins40 proteins were detected in cell lysates, and ACLP but not the ACLP-Ins40 was detected in the conditioned media. *B*, ACLP and ACLP-Ins40 C-terminal FLAG-tagged vectors were transfected into 3T3 fibroblasts, and ACLP was detected with a Cy3-conjugated anti-FLAG antibody. Cells were counterstained with DAPI (*blue*). *Arrows*, perinuclear ACLP expression. *C*, higher-magnification images of the ACLP-Ins40 protein revealed a pattern consistent with localization to the ER but with apparent absence in the Golgi apparatus indicated by a distinct "patch" adjacent to the nucleus (*arrow*). *D*, 3T3 mouse fibroblasts were transiently co-transfected with pCMV6-ACLP-WT-FLAG + XBP1u-EGFP or pCMV6-ACLP-Ins40-FLAG + XBP1u-EGFP plasmids and fixed with 2% paraformaldehyde after 24 h. Cells were stained with a Cy3-conjugated anti-FLAG antibody prior to counterstaining the nuclei with DAPI, mounting, and imaging. Perinuclear expression pattern of ACLP-WT and ACLP-Ins40 proteins in transfected cells is indicated by *arrows*. *E*, EGFP expression, indicative of ER stress was quantified from $n = 3$ independent transfection experiments ($p < 0.05$). Approximately 10 fields were imaged/condition in each experiment, and a total of 253 ACLP-WT and 320 ACLP-Ins40 cells were scored.

or ACLP-Ins40 + XBP1u-EGFP. After 24 h, cells were fixed, permeabilized, and stained with Cy3-conjugated anti-FLAG to detect transfected ACLP. Both ACLP and ACLP-Ins40 localized to the ER (Fig. 7*D*), and a significant increase in the ER stress reporter was detected in the ACLP Ins40-expressing cells (Fig. 7, *D* and *E*).

## Discussion

Here we show that ACLP secretion was tightly regulated by *N*-linked glycosylation and that the inhibition of glycosylation resulted in intracellular retention. We identified that modification of specific Asn residues (Asn-471 and Asn-1030) was necessary for secretion and also identified a previously unrecognized N-terminal proteolytic ACLP fragment. We studied a human EDS-causing ACLP mutation and determined that this protein was retained in the ER and induced ER stress measured with an XBP1-based ER stress reporter. To assess the contribution of ACLP to ECM mechanical properties, we generated wet-spun collagen ACLP composite fibers and by mechanical testing determined that the presence of ACLP enhanced the modulus, toughness, and tensile strength of the fibers. Thus, *N*-linked glycosylation of ACLP was necessary for secretion, and these findings contribute to the understanding of ACLP function in the ECM and the role of ACLP in EDS.

Accumulating evidence supports important functions for ACLP in multiple disease conditions, including lung, adipose tissue, and liver fibrosis (17, 20, 21, 31), wound healing (18), cancers (32–35), and neurodegeneration (36, 37). Significantly, multiple different mutations in the *AEBP1* gene, which encodes ACLP, cause a new variant of the connective tissue disorder EDS (7–11). Individuals with *AEBP1* mutations display clinical characteristics similar to symptoms of classical-like EDS and hypermobile EDS (8), and this new EDS subtype is designated EDS classic-like 2 (EDSCLL2). Although there are many similarities with the classical-like subtype, EDS symptoms caused by ACLP mutations can also fall under other subtypes. Additional work is needed to fully define the nature of the mutations in *AEBP1*/ACLP that result in null alleles or ablation of protein expression. Beyond the ACLP-Ins40 mutation described in this study, there is limited information characterizing the alleles that are null for protein expression or alleles that result in truncated or mutated proteins. For example, ACLP was not detected in fibroblasts isolated from an individual with the homozygous ACLP p.Arg440Serfs*3 mutation (8). This individual suffered from mitral valve prolapse and aortic root dilation, symptoms typically associated with vascular EDS (8). An additional patient presented with pectus excavatum and displayed spontaneous pneumothorax in adulthood, which is only seen in vascular EDS (11). Other individuals are predicted to be null for ACLP protein expression and suffer from severe osteopenia, severe joint and skin laxity, and disruptions in their facial features (7). In this case, it appears that the complete absence of ACLP caused many common clinical features of EDS to be experienced, whereas other truncating mutations result in kyphoscoliotic phenotypes (9). An additional mutation in ACLP encodes for a proline substitution in the carboxypeptidase-like domain that may disrupt both proper folding of ACLP and its secretion. The function of the catalytically inactive carboxypeptidase domain of ACLP is currently unknown. Reznik and Fricker (15) postulated that this domain could function as a binding domain rather than an active enzyme.

Additional studies are needed to determine whether the ACLP L642P point mutation in the carboxypeptidase domain discovered by Ritelli and colleagues (10) results in intracellular retention and ER stress similar to the ACLP-Ins40 mutation. We predict that mutations in ACLP will result in improper secretion and also hinder ACLP's ability to contribute to collagen assembly and mechanical properties, which are the underlying cause of EDS symptoms. It is also unclear whether ACLP has intracellular roles in collagen biosynthesis or chaperone-like function within the secretory pathway. Interestingly, the collagen chaperone, heat shock protein 47 (Hsp47), relieves ER stress in cancer cells (38). It is possible that ACLP has multiple functions in collagen biosynthesis and extracellular assembly.

The symptoms of EDS vary in severity based on subtype and extent of disease progression (39). A defining clinical feature is soft tissue fragility that affects almost every major organ system (40). EDS patients often display skin hyperextensibility and are prone to lacerations and bleeding even following minor abrasions. Vascular symptoms are the most concerning, as arterial or other spontaneous organ ruptures can result in sudden death (41). Loss of ACLP results in vascular defects in some individuals, and our prior work identified roles for ACLP in vascular remodeling (42). The mechanical testing studies of ACLP-collagen composite fibers (Fig. 5) support the concept that ACLP plays a structural role in collagen fiber stability. Additional research is needed to define the function of ACLP in collagen fibers; however, the significant decrease in diameter could indicate a change in structural arrangement that allows the fibers to condense more. ACLP's collagen-binding discoidin domain could contribute to collagen mechanical properties by acting like a protein bridge or cross-linker, as is observed for collagen V (43, 44).

The ACLP-Ins40 protein that was discovered in an EDS patient was retained intracellularly and not secreted. Due to the location of this mutation in the collagen-binding discoidin domain, we predicted that this protein would be secreted but not properly bind to collagen. However, when this protein was expressed in fibroblasts, it accumulated intracellularly and induced ER stress (Fig. 7). Therefore, it is likely that this mutation is a loss of function with respect to ECM assembly. The conserved glycosylation sites in the discoidin domain (mouse Asn-471 and Asn-519; Fig. 3*A*) and equivalent human sites (Asn-480 and Asn-528) are intact in the ACLP-Ins40 protein. Although it is possible that the ACLP-Ins40 protein glycosylation state is somehow altered by this mutation, the amino acid insertion in the discoidin domain is predicted to disrupt the highly conserved structure, which may be responsible for retention within the secretory pathway (Fig. 7). The amino acid insertion in the discoidin domain is predicted to disrupt the highly conserved structure, which may also be responsible for retention within the secretory pathway. The retention of ECM proteins and induction of ER stress have been observed with mutations in collagen III and VI, which like ACLP mutations cause connective tissue disease (29). In addition to ACLP discoidin mutations in EDS, there are a number of other diseases that result from mutations in discoidin domain–containing proteins, including retinoschisis (45), and in coagulation factors V and VIII (46). Similar to the pathogenic mutations in the retinoschisin 1 gene that result in the separation of the retinal layers or restinoschisis, the mutation in the ACLP-Ins40 protein includes the addition of 3 cysteine residues (8). It is possible that these cysteine residues result in aberrant folding, disulfide bond formation, protein aggregation, or intracellular retention. Additional research will need to test these hypotheses. Future studies will examine whether other branches of the unfolded protein response pathway, including activating transcription factor 6 (ATF6) and protein kinase R–like endoplasmic reticulum kinase (PERK) (47), are activated by mutations in the *AEBP1* gene that result in expressed proteins.

In addition to a role in ECM assembly, our previous work determined that ACLP signals via the TGF$\beta$ receptor complex (21), and Teratani *et al.* (17) determined that ACLP bound to and activated the LRP6/Frz8 signaling pathway, leading to $\beta$-catenin activation. Understanding the nature of the secreted ACLP protein is important to elucidate the details of these signaling pathways, and similar to our observations that secreted ACLP is glycosylated, Teratani *et al.* (17) also identified modifications in ACLP. Whether glycosylation is required for ACLP signaling activity, processing, and/or secretion remains to be determined. Furthermore, the nature of the proteolytic processing of ACLP in signaling is currently unknown, and the protease responsible for ACLP cleavage still remains to be identified. Interestingly, multiple bands of ACLP were observed in Western blotting analysis from human aortic aneurysms, which were proposed to be due to MMP9 or MMP12 activity (48). An additional predicted candidate is bone morphogenetic protein 1 (Bmp1), a secreted metalloproteinase, which provides the procollagen C-proteinase activity responsible for cleaving the C-propeptides from procollagens I-III (49, 50). Bmp1 null mouse embryos display herniation of the gut with a failure to close the ventral body wall, resulting in the embryos not being able to survive beyond birth (51). This phenotypic characteristic of the Bmp1 null mouse model has striking similarities to the ACLP-null mouse (18).

In this study, we have identified new mechanisms that regulate ACLP secretion and characterized an EDS-causing mutation. These data also have practical implications for studies generating recombinant forms of ACLP for *in vitro* testing in that alteration of glycosylation can cause intracellular retention. It remains to be determined whether other EDS-causing mutations in protein-coding domains of ACLP show similar intracellular retention, potentially resulting in loss of tissue integrity and collagen mechanics.

## Experimental procedures

Chemicals and reagents were obtained from Fisher unless otherwise indicated.

### Cell culture and treatments

Mouse aortic SMC were isolated from the aortas of adult mice as described previously (13). SMC were cultured in Dulbecco's modified Eagle's medium (DMEM) supplemented with 4.5 g/liter glucose, 1 mM sodium pyruvate, 1× nonessential amino acids, 100 units/ml penicillin, 100 μg/ml streptomycin, 2 mM L-glutamine (Corning Cellgro), and 20% fetal bovine serum

or bovine growth serum (Hyclone). SMC were routinely studied between passages 3 and 7. The Boston University School of Medicine institutional animal care and use committee approved all animal experiments. Human embryonic kidney 293 cells (AD-293, Stratagene 240085) and 3T3 fibroblasts (ATCC CRL-1658) were cultured in DMEM supplemented with 10% fetal bovine serum (Hyclone), 100 units/ml penicillin, 100 μg/ml streptomycin, and 2 mM L-glutamine. All cells were incubated at 37 °C in a humidified atmosphere containing 5% $CO_2$. In some studies, cells were treated with 2 μg/ml tunicamycin (Sigma, T7765) or 1 μM thapsigargin (Sigma, T9033) or with 50 μg/ml 2-phospho-L-ascorbic acid trisodium salt (Sigma, 49752).

### DNA constructs and site-directed mutagenesis

Mouse ACLP mammalian expression vectors with epitope tags are as described previously (13, 21). Restriction enzymes were purchased from New England Biolabs, and DNA fragments were purified using the QIAquick Gel Extraction Kit (Qiagen, 28706). Ligations were performed using the Quick Ligation Kit (New England Biolabs M2200S). To insert a FLAG epitope tag after the signal peptide cleavage site, two oligonucleotides that encode the FLAG epitope and NheI overhangs 5′-CTAGGAGATTACAAGGACGACGATGACAAGGCG-3′ and 5′-CTAGCGCCTTGTCATCGTCGTCCTTGTAATCTC-3′ were annealed and then ligated into NheI-digested pCEP-Pu/AC7, creating a vector with a single NheI site downstream of the signal sequence and FLAG epitope. Human ACLP expression plasmids pCMV6-hACLP-WT and epitope-tagged pCMV6-hACLP-WT-Myc-DDYK were obtained from Origene (RC207782 and SC309967). To generate ACLP expression plasmids harboring the EDS-causing human c.1470delC (p.Asn490_Met495delins(40)) mutation (designated ACLP-Ins40), RNA from patient fibroblasts (8) was converted into cDNA using the Maxima First Strand cDNA Synthesis Kit for RT-qPCR (Thermo Scientific, K164). The mutated region was then amplified using a forward primer harboring an EcoRI site and a reverse primer along with Q5 high-fidelity polymerase (New England Biolabs, E0555S): hACLPFwd (5′-GCGAATTCGCATGGCGGCCGTGCG-3′) and hACLPRev (5′-GCTGCGCACACACGTGGGTTCC-3′). This fragment was exchanged with the WT hACLP sequence using restriction enzyme digests and ligations in the pCMV6-hACLP and pCMV6-hACLP-Myc-DDYK plasmids to generate pCMVC6-hACLPIns40 and pCMV6-hACLPIns40-Myc-DDYK. To generate a sensor of XBP1-mediated ER stress, a fragment of unspliced XBP1 was generated by PCR using the forward primer that encodes a nuclear localization sequence NLS-XBP (5′-GCGAATTCGCCATGACCGCCCCCAAGAAGAAGCGGAAGGTGACGCTGGATCCTGACGAG-3′) and a reverse primer XBP1Rev (5′-CCGTCGACAAAAGGATATCAGACTC-3′). The PCR product was ligated into the EcoRI and SalI sites of pEGFP-N1 (Clontech). Subsequently, the EGFP-initiating methionine was mutated to leucine by PCR. In the absence of ER stress, EGFP will not be translated. With IRE1-mediated splicing (52) of the plasmid-derived mRNA, the methionine and nuclear localization sequence will be translated in frame with EGFP, enabling the monitoring of ER stress.

The ACLP sequence was analyzed using NetNGlyc software (53) for predicted sites of *N*-linked glycosylation. Four potential Asn amino acid residues (conserved in mouse and human) were predicted to undergo post-translational modification (Asn-471, Asn-519, Asn-913, and Asn-1030). Primers were designed (QuikChange Primer Design program (Stratagene/Agilent)) to individually mutate Asn residues to Gln (26). PCR site-directed mutagenesis was performed on pcDNA3.1 mACLP Myc/His plasmid using the Stratagene QuikChange method and Pfu Turbo DNA polymerase. All DNA constructs were verified by DNA sequencing.

### Transient transfection experiments

AD-293 cells and 3T3 fibroblasts were plated at ~150,000 cells/12-well plate or 200,000 cells/6-well plate and allowed to adhere overnight. Cells were transfected with 1-2 μg of plasmid DNA using TransIT-2020 or TransIT-293 reagent (Mirus Bio, MIR 5404 and MIR 2704) according to the instructions of the manufacturer in Opti-MEM reduced serum medium (Thermo Fisher, 31985088) supplemented with Gluta-MAX (Invitrogen). Transfection efficiency was monitored by transfection of pMax-GFP (Lonza) in separate wells and was routinely between 30 and 50%.

### Immunofluorescence

Transfected 3T3 fibroblasts were grown on 4-well chamber slides with removable chambers (Thermo Fisher, 154453). Cells were washed twice with PBS and fixed with 4% paraformaldehyde in PBS for 15 min. Cells were permeabilized in PBS + 0.1% Triton X-100 (PBST) for 5 min, washed twice more in PBS, and blocked in 3% BSA PBST for 1 h. Cells were then stained with mouse anti-FLAG M2-Cy3 Ab (Sigma, A9594) at a 1:100 dilution and kept in the dark for 1 h. Slides were then washed twice in PBST and twice in PBS. Slides were spun down to dry in 50-ml tubes (75 × *g* for 3 min) and mounted with ProLong Diamond Antifade Mountant with DAPI (Thermo Fisher, P36962). Slides were imaged using a Zeiss fluorescent microscope and ZEN software. Microscope settings and exposure times were kept constant for each sample within a single experiment. For each independent experiment, ~10 fields were captured per condition, and images were analyzed with Fiji software. ACLP and XBP reporter (GFP)-positive cells were counted manually to generate a single value from each condition. Statistical significance was determined using an unpaired Student's *t* test.

### Protein extraction and Western blot analysis

Total cell lysates were prepared from cell layers as described previously (13) using (25 mM Tris, pH 7.4, 50 mM NaCl, 0.5% sodium deoxycholate, 2% Nonidet P-40, 0.2% SDS) with 1× Complete protease inhibitors (Roche Applied Science, 04693124001). Protein concentrations were measured using the BCA Protein Assay Kit (Pierce–Thermo Scientific, 23227) according to the manufacturer's instructions. Secreted protein/conditioned medium was collected from cells incubated in serum-free DMEM supplemented with 100 units/ml penicillin, 100 μg/ml streptomycin, and 2 mM L-

glutamine. Conditioned media samples were cleared of cellular debris by centrifugation at 1,000 × *g* for 10 min at 4 °C and then concentrated ~40-80-fold using 10,000 molecular weight cut-off Amicon Ultra Centrifugal Filters (Millipore Sigma). Protein samples were fractionated by either 6% or 4–20% gradient SDS-polyacrylamide gels (Novex, Invitrogen) and transferred to nitrocellulose membranes (Whatman Protran, BA85). Primary antibodies used were the fully characterized rabbit anti-ACLP (1:4,000) (13), mouse anti-pan-actin (1:4,000) (Millipore, MS1295P0), rabbit anti-FLAG (1:1,000) (Cell Signaling, 2638), mouse anti-c-Myc 9E10 (1:1,000) (Santa Cruz Biotechnology, Inc., SC-40), followed by detection with horseradish peroxidase–conjugated secondary antibodies: donkey anti-rabbit and sheep anti-mouse (1:4,000) (GE Healthcare). Signal was detected by enhanced chemiluminescence (Pierce) and exposure to film or imaged with a Bio-Rad ChemiDoc imaging system with Quantity One 1-D analysis software. All blots are representative of at least three independent experiments.

### *Glycosidase treatment*

Total cell lysates and concentrated media samples were treated with specific proteoglycan-cleaving enzymes and buffers acquired from New England Biolabs. A standard reaction consisted of a 20-μl volume. Briefly, 1 μl of 10× glycoprotein-denaturing buffer was added to 9 μl of total cell lysate or cell media samples. For some experiments, media samples were diluted 1:5 in 1× PBS. The samples were denatured at 99 °C for 10 min Next, the buffering reagents 10× G7 buffer, 10× G1 buffer, 10% Nonidet P-40, and/or 1× PBS were added according to the instructions of the manufacturer. Samples were then either individually digested or double-digested with the following enzymes: 500 units/μl PNGase F (P0704S) and 50 units/μl α2-3,6,8 neuraminidase (P0720S) (New England Biolabs). All final assembled enzymatic reactions were incubated at 37 °C for 1-2 h prior to analysis by Western blotting as described above. All blots are representative of at least three independent experiments.

### *Wet-spun ECM fibers and mechanical measurements*

Collagen I and collagen I + ACLP composite fibers were generated using methods described previously (27, 28, 54). A protein solution was mixed consisting of 7 mg/ml rat tail collagen I (Corning, 354249), 233 μg/ml (3% by weight) recombinant ACLP (prepared as described (21)) or PBS, 10% by volume, 1 M NaOH, and 7.5% by volume PBS with $Ca^{2+}$ and $Mg^{2+}$. Solutions were loaded into a Hamilton 250-μl gas-tight syringe and extruded at 2.5 μl/min through the syringe's 23-gauge needle into a coagulation bath containing 100% isopropyl alcohol, where the fibers formed. Fibers were attached to a sacrificial frame with double-sided tape and secured with epoxy. Fibers were imaged with an Olympus IX81 microscope, and the diameter was determined by measuring the diameter at nine points along the fiber, and these values were averaged to give a value for each fiber. The fibers on the frames were loaded into an Instron microtester with a 5-newton load cell, the sides of the frames were melted away with a soldering iron, and a tensile test was performed at a strain rate of 0.01 $s^{-1}$. Data were analyzed in MATLAB.

## Data availability

All data are contained within this article. Requests for reagents and additional information on experimental procedures will be provided by Matthew D. Layne (mlayne@bu.edu).

*Acknowledgments*—We thank Robert Shine for generating the XBP-EGFP vector and Rose Zhao for designing the ACLP-Ins40 expression vector. We thank Paldeep Atwal, Patrick Blackburn, Joseph Zaia, and Barbara Schreiber for helpful discussions. We thank the Biointerface Technologies Core Facility of Boston University's Biomedical Engineering Department for use of their Instron microtester.

*Author contributions*—N. V., W. J. M., G. A. H., J. Y. W., M. L. S., and M. D. L. conceptualization; N. V., W. J. M., G. A. H., B. R., V. D., and M. D. L. investigation; N. V., W. J. M., G. A. H., J. Y. W., M. L. S., and M. D. L. methodology; N. V., W. J. M., and M. D. L. writing-original draft; N. V., W. J. M., G. A. H., B. R., V. D., J. Y. W., M. L. S., and M. D. L. writing-review and editing; J. Y. W., M. L. S., and M. D. L. supervision; M. D. L. funding acquisition; M. D. L. project administration.

*Funding and additional information*—This work was supported in part by National Institutes of Health Grant HL078869 (to M. D. L.). G. A. H. was supported by National Institutes of Health Graining Grants T32 GM008764 and F31 HL151082. The content is solely the responsibility of the authors and does not necessarily represent the official views of the National Institutes of Health.

*Conflict of interest*—The authors declare that they have no conflicts of interest with the contents of this article.

*Abbreviations*—The abbreviations used are: ECM, extracellular matrix; EDS, Ehlers–Danlos syndrome; EDSCLL2, EDS classic-like 2; ACLP, aortic carboxypeptidase-like protein; TGF, transforming growth factor; SMC, smooth muscle cells; PNGase F, peptide:N-glycosidase F; EGFP, enhanced GFP; DMEM, Dulbecco's modified Eagle's medium; DAPI, 4′,6-diamidino-2-phenylindole.

## References

1. Hynes, R. O., and Naba, A. (2012) Overview of the matrisome—an inventory of extracellular matrix constituents and functions. *Cold Spring Harb. Perspect. Biol.* **4,** a004903 CrossRef Medline
2. Finch-Edmondson, M., and Sudol, M. (2016) Framework to function: mechanosensitive regulators of gene transcription. *Cell Mol. Biol. Lett.* **21,** 28 CrossRef Medline
3. Lampi, M. C., and Reinhart-King, C. A. (2018) Targeting extracellular matrix stiffness to attenuate disease: from molecular mechanisms to clinical trials. *Sci. Transl. Med.* **10,** eaao0475 CrossRef
4. Tschumperlin, D. J., Ligresti, G., Hilscher, M. B., and Shah, V. H. (2018) Mechanosensing and fibrosis. *J. Clin. Invest.* **128,** 74–84 CrossRef Medline
5. Malfait, F., Francomano, C., Byers, P., Belmont, J., Berglund, B., Black, J., Bloom, L., Bowen, J. M., Brady, A. F., Burrows, N. P., Castori, M., Cohen, H., Colombi, M., Demirdas, S., De Backer, J., *et al.* (2017) The 2017 international classification of the Ehlers-Danlos syndromes. *Am. J. Med. Genet. C Semin. Med. Genet.* **175,** 8–26 CrossRef Medline

6. Vanakker, O., Callewaert, B., Malfait, F., and Coucke, P. (2015) The Genetics of soft connective tissue disorders. *Annu. Rev. Genomics Hum. Genet.* **16,** 229–255 CrossRef Medline
7. Alazami, A. M., Al-Qattan, S. M., Faqeih, E., Alhashem, A., Alshammari, M., Alzahrani, F., Al-Dosari, M. S., Patel, N., Alsagheir, A., Binabbas, B., Alzaidan, H., Alsiddiky, A., Alharbi, N., Alfadhel, M., Kentab, A., *et al.* (2016) Expanding the clinical and genetic heterogeneity of hereditary disorders of connective tissue. *Hum. Genet.* **135,** 525–540 CrossRef Medline
8. Blackburn, P. R., Xu, Z., Tumelty, K. E., Zhao, R. W., Monis, W. J., Harris, K. G., Gass, J. M., Cousin, M. A., Boczek, N. J., Mitkov, M. V., Cappel, M. A., Francomano, C. A., Parisi, J. E., Klee, E. W., Faqeih, E., *et al.* (2018) Bi-allelic alterations in AEBP1 lead to defective collagen assembly and connective tissue structure resulting in a variant of Ehlers-Danlos syndrome. *Am. J. Hum. Genet.* **102,** 696–705 CrossRef Medline
9. Hebebrand, M., Vasileiou, G., Krumbiegel, M., Kraus, C., Uebe, S., Ekici, A. B., Thiel, C. T., Reis, A., and Popp, B. (2019) A biallelic truncating AEBP1 variant causes connective tissue disorder in two siblings. *Am. J. Med. Genet. A* **179,** 50–56 CrossRef Medline
10. Ritelli, M., Cinquina, V., Venturini, M., Pezzaioli, L., Formenti, A. M., Chiarelli, N., and Colombi, M. (2019) Expanding the clinical and mutational spectrum of recessive *AEBP1*-related classical-like Ehlers-Danlos syndrome. *Genes (Basel)* **10,** 135 CrossRef Medline
11. Syx, D., De Wandele, I., Symoens, S., De Rycke, R., Hougrand, O., Voermans, N., De Paepe, A., and Malfait, F. (2019) Bi-allelic AEBP1 mutations in two patients with Ehlers-Danlos syndrome. *Hum. Mol. Genet.* **28,** 1853–1864 CrossRef Medline
12. He, G. P., Muise, A., Li, A. W., and Ro, H. S. (1995) A eukaryotic transcriptional repressor with carboxypeptidase activity. *Nature* **378,** 92–96 CrossRef Medline
13. Layne, M. D., Endege, W. O., Jain, M. K., Yet, S. F., Hsieh, C. M., Chin, M. T., Perrella, M. A., Blanar, M. A., Haber, E., and Lee, M. E. (1998) Aortic carboxypeptidase-like protein, a novel protein with discoidin and carboxypeptidase-like domains, is up-regulated during vascular smooth muscle cell differentiation. *J. Biol. Chem.* **273,** 15654–15660 CrossRef Medline
14. Tumelty, K. E., and Layne, M. D. (2013) Adipocyte enhancer binding protein 1 and aortic carboxypeptidase-like protein. in *Handbook of Proteolytic Enzymes* (Rawlings, N. D., and Salvesen, G. eds.) 3rd Ed., pp. 1352–1357, Elsevier, Amsterdam
15. Reznik, S. E., and Fricker, L. D. (2001) Carboxypeptidases from A to Z: implications in embryonic development and Wnt binding. *Cell Mol. Life Sci.* **58,** 1790–1804
16. Abderrahim-Ferkoune, A., Bezy, O., Astri-Roques, S., Elabd, C., Ailhaud, G., and Amri, E. Z. (2004) Transdifferentiation of preadipose cells into smooth muscle-like cells: role of aortic carboxypeptidase-like protein. *Exp. Cell Res.* **293,** 219–228 CrossRef Medline
17. Teratani, T., Tomita, K., Suzuki, T., Furuhashi, H., Irie, R., Nishikawa, M., Yamamoto, J., Hibi, T., Miura, S., Minamino, T., Oike, Y., Hokari, R., and Kanai, T. (2018) Aortic carboxypeptidase-like protein, a WNT ligand, exacerbates nonalcoholic steatohepatitis. *J. Clin. Invest.* **128,** 1581–1596 CrossRef Medline
18. Layne, M. D., Yet, S. F., Maemura, K., Hsieh, C. M., Bernfield, M., Perrella, M. A., and Lee, M. E. (2001) Impaired abdominal wall development and deficient wound healing in mice lacking aortic carboxypeptidase-like protein. *Mol. Cell Biol.* **21,** 5256–5261 CrossRef Medline
19. Ith, B., Wei, J., Yet, S. F., Perrella, M. A., and Layne, M. D. (2005) Aortic carboxypeptidase-like protein is expressed in collagen-rich tissues during mouse embryonic development. *Gene Expr. Patterns* **5,** 533–537 CrossRef Medline
20. Schissel, S. L., Dunsmore, S. E., Liu, X., Shine, R. W., Perrella, M. A., and Layne, M. D. (2009) Aortic carboxypeptidase-like protein is expressed in fibrotic human lung and its absence protects against bleomycin-induced lung fibrosis. *Am. J. Pathol.* **174,** 818–828 CrossRef Medline
21. Tumelty, K. E., Smith, B. D., Nugent, M. A., and Layne, M. D. (2014) Aortic carboxypeptidase-like protein (ACLP) enhances lung myofibroblast differentiation through transforming growth factor $\beta$ receptor-dependent and -independent pathways. *J. Biol. Chem.* **289,** 2526–2536 CrossRef Medline
22. Jager, M., Lee, M. J., Li, C., Farmer, S. R., Fried, S. K., and Layne, M. D. (2018) Aortic carboxypeptidase-like protein enhances adipose tissue stromal progenitor differentiation into myofibroblasts and is upregulated in fibrotic white adipose tissue. *PLoS ONE* **13,** e0197777 CrossRef Medline
23. Van Robertson, W. B., and Schwartz, B. (1953) Ascorbic acid and the formation of collagen. *J. Biol. Chem.* **201,** 689–696 Medline
24. Ricard-Blum, S. (2011) The collagen family. *Cold Spring Harb. Perspect. Biol.* **3,** a004978 CrossRef Medline
25. Price, N. P., and Tsvetanova, B. (2007) Biosynthesis of the tunicamycins: a review. *J. Antibiot. (Tokyo)* **60,** 485–491 CrossRef Medline
26. Hoosdally, S. J., Andress, E. J., Wooding, C., Martin, C. A., and Linton, K. J. (2009) The human scavenger receptor CD36: glycosylation status and its role in trafficking and function. *J. Biol. Chem.* **284,** 16277–16288 CrossRef Medline
27. Jacobsen, M. M., Li, D., Gyune Rim, N., Backman, D., Smith, M. L., and Wong, J. Y. (2017) Silk-fibronectin protein alloy fibres support cell adhesion and viability as a high strength, matrix fibre analogue. *Sci. Rep.* **7,** 45653 CrossRef Medline
28. Bradshaw, M. J., Hoffmann, G. A., Wong, J. Y., and Smith, M. L. (2019) Fibronectin fiber creep under constant force loading. *Acta Biomater.* **88,** 78–85 CrossRef Medline
29. Boot-Handford, R. P., and Briggs, M. D. (2010) The unfolded protein response and its relevance to connective tissue diseases. *Cell Tissue Res.* **339,** 197–211 CrossRef Medline
30. Merksamer, P. I., and Papa, F. R. (2010) The UPR and cell fate at a glance. *J. Cell Sci.* **123,** 1003–1006 CrossRef Medline
31. Gerhard, G. S., Hanson, A., Wilhelmsen, D., Piras, I. S., Still, C. D., Chu, X., Petrick, A. T., and DiStefano, J. K. (2019) AEBP1 expression increases with severity of fibrosis in NASH and is regulated by glucose, palmitate, and miR-372-3p. *PLoS ONE* **14,** e0219764 CrossRef Medline
32. Xing, Y., Zhang, Z., Chi, F., Zhou, Y., Ren, S., Zhao, Z., Zhu, Y., and Piao, D. (2019) AEBP1, a prognostic indicator, promotes colon adenocarcinoma cell growth and metastasis through the NF-$\kappa$B pathway. *Mol. Carcinog.* **58,** 1795–1808 CrossRef Medline
33. Li, S., Li, C., and Fang, Z. (2018) MicroRNA 214 inhibits adipocyte enhancer-binding protein 1 activity and increases the sensitivity of chemotherapy in colorectal cancer. *Oncol. Lett.* **17,** 55–62 CrossRef Medline
34. Li, S., Juan, C. X., Feng, A. M., Bian, H. L., Liu, W. D., Zhang, G. Q., Wang, C. Z., Cao, Q., and Zhou, G. P. (2019) Attenuating the abnormally high expression of AEBP1 suppresses the pathogenesis of childhood acute lymphoblastic leukemia via p53-dependent signaling pathway. *Eur. Rev. Med. Pharmacol. Sci.* **23,** 1184–1195 CrossRef Medline
35. Liu, J. Y., Jiang, L., Liu, J. J., He, T., Cui, Y. H., Qian, F., and Yu, P. W. (2018) AEBP1 promotes epithelial-mesenchymal transition of gastric cancer cells by activating the NF-$\kappa$B pathway and predicts poor outcome of the patients. *Sci. Rep.* **8,** 11955 CrossRef Medline
36. Shijo, M., Honda, H., Suzuki, S. O., Hamasaki, H., Hokama, M., Abolhassani, N., Nakabeppu, Y., Ninomiya, T., Kitazono, T., and Iwaki, T. (2018) Association of adipocyte enhancer-binding protein 1 with Alzheimer's disease pathology in human hippocampi. *Brain Pathol.* **28,** 58–71 CrossRef Medline
37. Piras, I. S., Krate, J., Delvaux, E., Nolz, J., De Both, M. D., Mastroeni, D. F., Serrano, G. E., Sue, L. I., Beach, T. G., Coleman, P. D., and Huentelman, M. J. (2019) Association of AEBP1 and NRN1 RNA expression with Alzheimer's disease and neurofibrillary tangle density in middle temporal gyrus. *Brain Res.* **1719,** 217–224 CrossRef Medline
38. Yoneda, A., Sakai-Sawada, K., Minomi, K., and Tamura, Y. (2020) Heat shock protein 47 maintains cancer cell growth by inhibiting the unfolded protein response transducer IRE1$\alpha$. *Mol. Cancer Res.* **18,** 847–858 CrossRef Medline
39. Beighton, P., De Paepe, A., Steinmann, B., Tsipouras, P., and Wenstrup, R. J. (1998) Ehlers-Danlos syndromes: revised nosology, Villefranche, 1997. Ehlers-Danlos National Foundation (U.S.A.) and Ehlers-Danlos Support Group (UK). *Am. J. Med. Genet.* **77,** 31–37 CrossRef Medline
40. Malfait, F., and De Paepe, A. (2014) The Ehlers-Danlos syndrome. *Adv. Exp. Med. Biol.* **802,** 129–143 CrossRef Medline
41. Pepin, M., Schwarze, U., Superti-Furga, A., and Byers, P. H. (2000) Clinical and genetic features of Ehlers-Danlos syndrome type IV, the vascular type. *N. Engl. J. Med.* **342,** 673–680 CrossRef Medline

42. Layne, M. D., Yet, S. F., Maemura, K., Hsieh, C. M., Liu, X., Ith, B., Lee, M. E., and Perrella, M. A. (2002) Characterization of the mouse aortic carboxypeptidase-like protein promoter reveals activity in differentiated and dedifferentiated vascular smooth muscle cells. *Circ. Res.* **90,** 728–736 CrossRef Medline
43. Connizzo, B. K., Freedman, B. R., Fried, J. H., Sun, M., Birk, D. E., and Soslowsky, L. J. (2015) Regulatory role of collagen V in establishing mechanical properties of tendons and ligaments is tissue dependent. *J. Orthop. Res.* **33,** 882–888 CrossRef Medline
44. Sun, M., Chen, S., Adams, S. M., Florer, J. B., Liu, H., Kao, W. W., Wenstrup, R. J., and Birk, D. E. (2011) Collagen V is a dominant regulator of collagen fibrillogenesis: dysfunctional regulation of structure and function in a corneal-stroma-specific Col5a1-null mouse model. *J. Cell Sci.* **124,** 4096–4105 CrossRef Medline
45. den Dunnen, J. T. (1998) Functional implications of the spectrum of mutations found in 234 cases with X-linked juvenile retinoschisis. The Retinoschisis Consortium. *Hum. Mol. Genet.* **7,** 1185–1192 CrossRef Medline
46. Fuentes-Prior, P., Fujikawa, K., and Pratt, K. P. (2002) New insights into binding interfaces of coagulation factors V and VIII and their homologues lessons from high resolution crystal structures. *Curr. Protein Pept. Sci.* **3,** 313–339 CrossRef Medline
47. Walter, P., and Ron, D. (2011) The unfolded protein response: from stress pathway to homeostatic regulation. *Science* **334,** 1081–1086 CrossRef Medline
48. Didangelos, A., Yin, X., Mandal, K., Saje, A., Smith, A., Xu, Q., Jahangiri, M., and Mayr, M. (2011) Extracellular matrix composition and remodeling in human abdominal aortic aneurysms: a proteomics approach. *Mol. Cell. Proteomics* **10,** M111.008128 CrossRef Medline
49. Hopkins, D. R., Keles, S., and Greenspan, D. S. (2007) The bone morphogenetic protein 1/Tolloid-like metalloproteinases. *Matrix Biol.* **26,** 508–523 CrossRef Medline
50. Trackman, P. C. (2005) Diverse biological functions of extracellular collagen processing enzymes. *J. Cell. Biochem.* **96,** 927–937 CrossRef Medline
51. Suzuki, N., Labosky, P. A., Furuta, Y., Hargett, L., Dunn, R., Fogo, A. B., Takahara, K., Peters, D. M., Greenspan, D. S., and Hogan, B. L. (1996) Failure of ventral body wall closure in mouse embryos lacking a procollagen C-proteinase encoded by Bmp1, a mammalian gene related to *Drosophila* tolloid. *Development* **122,** 3587–3595 Medline
52. Calfon, M., Zeng, H., Urano, F., Till, J. H., Hubbard, S. R., Harding, H. P., Clark, S. G., and Ron, D. (2002) IRE1 couples endoplasmic reticulum load to secretory capacity by processing the XBP-1 mRNA. *Nature* **415,** 92–96 CrossRef Medline
53. Blom, N., Sicheritz-Pontén, T., Gupta, R., Gammeltoft, S., and Brunak, S. (2004) Prediction of post-translational glycosylation and phosphorylation of proteins from the amino acid sequence. *Proteomics* **4,** 1633–1649 CrossRef Medline
54. Teulé, F., Cooper, A. R., Furin, W. A., Bittencourt, D., Rech, E. L., Brooks, A., and Lewis, R. V. (2009) A protocol for the production of recombinant spider silk-like proteins for artificial fiber spinning. *Nat. Protoc.* **4,** 341–355 CrossRef Medline